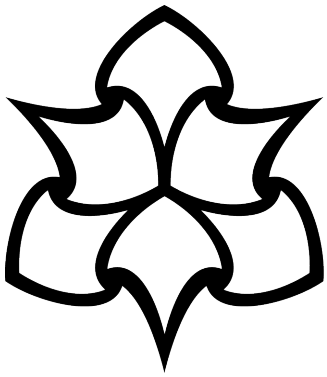

Facile synthesis of cellulose microfibers supported palladium nanospindles on graphene oxide for selective detection of dopamine in pharmaceutical and biological samples

Selvakumar Palanisamy[a,b*], Vijaylakshmi Velusamy[b**], Sukanya Ramaraj[c], Shih-Wen Chen[a], Thomas C.K. Yang[b***], Sridharan Balu[c], Craig E Banks[d]

[a]Department of Chemical Engineering, National Taipei University of Technology, No. 1, Section 3, Chung-Hsiao East Road, Taipei City, Taiwan

[b]Division of Electrical and Electronic Engineering, School of Engineering, Manchester Metropolitan University, Chester Street, Manchester M1 5GD, United Kingdom

[c]Electroanalysis and Bioelectrochemistry Lab, Department of Chemical Engineering and Biotechnology, National Taipei University of Technology, No. 1, Section 3, Chung-Hsiao East Road, Taipei 106, Taiwan

[d]School of Science and Environment, Manchester Metropolitan University, Chester Street, Manchester M1 5GD, United Kingdom

Corresponding authors

** S. Palanisamy (prmselva@gmail.com; prmselva@mail.ntut.edu.tw)

** V. Velusamy (V.Velusamy@mmu.ac.uk)

** T.C.K. Yang (ckyang@mail.ntut.edu.tw)

Abstract

The cost-effective synthesis of novel functional nanomaterials has received significant attention in the physical and chemical sciences due to their improved surface area, high catalytic activity along with unique morphological features. This paper reports a facile and eco-friendly synthesis of spindle-like palladium nanostructures (PdSPs) on graphene oxide-cellulose microfiber (GO-CMF) composite for the first time. The GO-CMF/PdSPs composite was synthesized by an electrochemical method without the use of additional surfactants and capping agents. The synthesized materials were characterized and confirmed by using transmission electron microscopy, high-resolution scanning electron microscopy, X-ray diffraction spectroscopy, Raman spectroscopy and Fourier-transform infrared spectroscopy. As-synthesized GO-CMF/PdSPs composite modified electrode was used as a selective electrocatalyst for the oxidation of dopamine (DA). The electrochemical redox behaviors of DA were investigated using cyclic voltammetry (CV). The CV results revealed that the GO-CMF/PdSPs composite modified electrode has 10 folds enhanced oxidation current response to DA than GO, PdSPs and GO-CMF modified GCEs. Under optimized conditions, the GO-CMF/PdSPs composite sensor exhibits a linear response to DA in the concentration range from 0.3 to 196.3 μM with the lower detection limit of 23 nM. The nanocomposite electrode also shows promising features towards the reliable and selective detection of DA, which includes high stability, reproducibility and high selectivity towards the commonly interfering species such as ascorbic acid, uric acid, and dihydroxybenzene isomers. The sensor was successfully tested for the real-time detection of DA in the commercial DA injections and human serum samples.

Keywords: Graphene oxide; cellulose microfibers; palladium nanospindles; electrochemical synthesis; dopamine; biological applications

1. Introduction

In recent decades, the synthesis of nanocomposite materials with improved physicochemical properties has received much attention in different disciplines including materials and environmental sciences [**1–4**]. In specific, the composites of graphene-related materials have found profound interest due to their unique physicochemical properties with distinct morphological features [**5**]. Among different graphenoids, graphene oxide (GO) is 2D materials with tunable functionalities, has been emerged as a building block of graphene and graphene-based composites [**6, 7**]. Due to the presence of reactive oxygen functional groups, GO has been used as an essential additive or performance enhanced material for nanocomposites [**8–10**]. The practical application of pristine GO is limited due to its poor electrical conductivity which arises from the covalent oxygenated functional groups on the edge and basal planes [**10**]. However, GO has been used as an ideal material for intercalation of biopolymers and metal nanoparticles due to its excellent biocompatibility and amphiphilicity [**11**]. It is reported that cellulosic materials have a strong tendency of bonding with semi-conductive materials like GO, resulting in improved physicochemical properties of GO [**12, 13**]. Among different cellulosic materials, cellulose fibers (CMF) has many distinct advantages such as excellent biocompatibility, high porosity, and excellent hydrophilicity, thus result into the excellent film-forming ability and enhanced conductivity with GO, the reduced form of GO nanosheets and graphene [**14**]. Also, we have recently reported that CMF is an ideal material for the synthesis of stable composites with reduced graphene oxide and graphene [**15–18**]. The resulting composite materials showed enhanced physicochemical properties than pristine graphene. Hence, in the present work, we have prepared GO and CMF composite by a simple sonication method, and the spindles-like palladium (PdSPs) nanostructures were decorated on GO-CMF composite by electrochemical method. The integration of PdSPs prevented the self-aggregation of GO and improved the stability of GO-CMF composite.

Dopamine (DA) is one of significant catecholamines and played a vital role as a neurotransmitter in the central nervous system (CNS) of human and multicellular animals brain [**19**]. DA also acts as a local

chemical messenger in the mammalian body [**20**]. The dysfunctions DA in CNS leads to the range of neurological and psychiatric disorders including but not limited to Parkinson's disease, attention deficit, schizophrenia, and attention deficit hyperactivity disorder [**21, 22**]. Hence, the real-time detection of DA in biological fluids is of interest, Different analytical methods have been reported for accurate detection of DA, yet the electrochemical methods are widely employed for the sensitive detection of DA due to its highly electroactive in nature [**23**]. However, the unmodified graphite and glassy carbon electrodes are not feasible for real-time detection of DA due to their poor selectivity arising from the fowling of signals by the oxidized products of DA [**24**]. To address these problems, the chemically modified electrodes have been widely employed for sensitive and selective detection of DA which includes carbon nanomaterials, metal alloy nanoparticles, conducting polymers, ionic liquids, redox-active enzymes and organometallic compounds [**25, 26**]. Furthermore, different strategies or pretreatments have been used on the electrode surface to improve the sensitivity and selectivity of DA [**27, 28**].

Recent studies showed that palladium (Pd) nanomaterials had been widely employed as an electrode material for electrochemical sensing of different compounds including but not limited to DA [**29, 30**], ascorbic acid [**29**], paracetamol [**31**], H_2O_2 [**22**], glucose [**33**], and nitrophenol [**34**]. Furthermore, Pd nanocomposite modified electrodes showed high sensitivity and selectivity to the investigated compounds than pristine nano Pd. It is reported earlier that the Pd nanoparticles (PdNPs) modified electrode has high electro-oxidation ability towards DA at lower potentials [**29, 30, 35, 36**]. However, the selective detection of DA using PdNPs is still problematic in biological samples due to the co-existence of DA with ascorbic acid (AA) [**29**]. The integration of GO can address the selectivity with nano Pd since DA can be strongly attracted by negatively charged GO than AA [**37**]. Hence, in the present work, we report the synthesis of spindle-like Pd nanostructures (PdSPs) on GO for selective DA biosensor applications for the first time. A facile electrochemical synthesis method was used for the synthesis of CMF supported GO/PdSPs (GO-CMF/PdSPs) composite. The high miscible nature CMF on GO which results in the formation of PdNPs rather than PdNPs on the composite. The as-prepared GO-CMF/PdSPs

composite modified electrode is further used for the DA electrochemical sensor applications. Compared with GO, PdSPs and GO-CMF modified electrodes, the GO-CMF/PdSPs composite modified electrode shows an enhanced redox electrochemical behavior to DA with improved sensitivity.

2. Experimental

2.1. Electrodes fabrication and methods

The Hummers' method was used for the oxidation of pristine graphite (<20 μm, synthetic from Sigma-Aldrich) to graphite oxide [**38**]. The stable GO solution was prepared by sonication (Bransonic Ultrasonic Bath with an operating frequency of 40 kHz and ultrasonic power output of 250 W) of synthesized graphite oxide (0.5 mg mL^{-1}) with the ultrapure doubly distilled (DD) water (resistivity >18.2 MΩ·cm at 25 °C). To prepare GO-CMF composite, first, the CMF (medium ranged microfibers from Sigma-Aldrich) solution was prepared by the addition of CMF (5 mg mL^{-1}) into the DD water and followed by sonication about 1 h. The graphite oxide powder (0.5 mg mL^{-1}) was added into the CMF solution (2 mL). The resulting mixture was bath sonicated (30 min) until the apparent suspension of GO-CMF composite obtained. About 0.1 mM $PdCl_2$ (assay 99.999% from Sigma-Aldrich) was added into the GO-CMF composite suspension and sonicated for 15 min. Then, 8 μL of the as-prepared composite solution was dropped on pre-cleaned GCE and air dried. The as-prepared Pd ions adsorbed GO-CMF composite modified electrode (**Scheme 1**) was then transferred into the electrochemical cell containing the pH 3 solution and applied a constant potential of −0.4 V for 200 s. The fabricated GO-CMF/PdSPs composite modified electrode was gently rinsed with DD water and dried in an air oven. For comparison, PdSPs/CMF, GO, and GO-CMF modified electrodes were prepared. To prepare the PdSPs/CMF modified electrode, first, the 0.1 mM $PdCl_2$ was added into the CMF solution and sonicated for 15 min. Then, 8 μL of the as-prepared composite solution was dropped on GCE and air dried. The resulting electrode was immersed into the pH 3 and applied a constant potential of −0.4 V for 200 s. The fabricated electrode was gently rinsed with DD water to remove the loosely attached Pd ions. The fabricated terminal electrode is named

as PdSPs/CMF modified electrode. The GO and GO-CMF modified electrodes were prepared by drop coating optimum amount (8 µL) of GO and GO-CMF on unmodified GCE. The schematic illustration of the electrochemical synthesis of PdNPs and GO-CMF/PdSPs composite are shown in **Scheme 1**. The electrochemical measurements were performed in N_2 saturated pH 7.0 unless otherwise stated. The fabricated electrodes were stored in a dry condition when not in use. The 0.1 M of DA and interfering compounds stock solutions were prepared using DD water, and 0.1 M phosphate buffer pH 7.0 (PBS) was used as a supporting electrolyte for electrochemical experiments. The human blood serum samples (from the valley biomedical, Taiwan product & services, Inc) were prepared by diluting with pH 7.0. The DA hydrochloride injection (1.6 mg mL^{-1}) stock solutions were prepared by diluting with pH 7.0 to desired concentrations. The experiments were conducted at room temperature (25 ± 2 °C) unless otherwise stated.

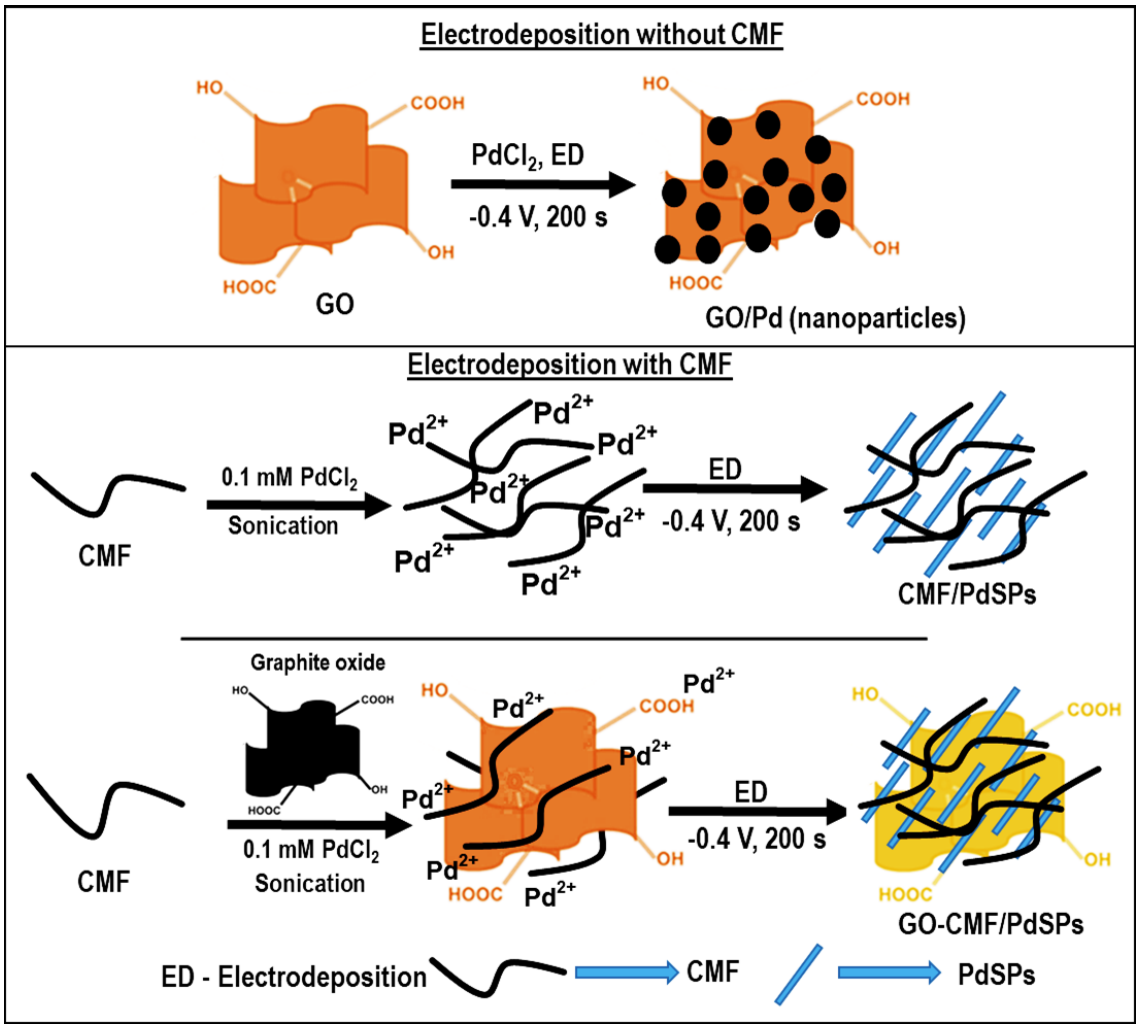

Scheme 1 Schematic illustration of the electrochemical synthesis of GO-CMF/PdSPs composite and PdSPs.

The surface morphological characterizations of the as-prepared materials were analyzed by the Hitachi S-4300SE/N High-Resolution Schottky Analytical VP scanning electron microscope and JEOL JEM2100F (Peabody, MA, USA) transmission electron microscope. Thermal gravimetric analysis (TGA) of the materials was carried out using STA7300 thermal analysis system from HITACHI. Raman spectra of the materials were acquired using Dong Woo 500i Raman spectrometer. The X-Ray diffraction (XRD) spectrum of the as-prepared composite coated indium tin oxide (ITO) glass was acquired using PANanalytical X'Pert PRO XRD, Almelo, Netherlands. The interactions between GO and CMF and the formation of the composites were analyzed using Fourier transform infrared (FTIR) spectroscopy and was done by JASCO FTIR-6600 spectrometer. Cyclic voltammetry and differential pulse voltammetry (DPV) experiments were carried out using CHI900 electrochemical scanning microscope (CH Instruments). A standard three-electrode setup (GCE, saturated Ag|AgCl and Pt wire) was used for electrochemical studies unless otherwise stated.

3. Results and discussion

3.1. Characterizations of as-prepared materials

The formation of GO-CMF/PdSPs composite is further confirmed by XRD, and the corresponding XRD spectrum of GO-CMF/PdSPs composite coated ITO glass is shown in **Fig. 1A**. It can be seen that the three diffraction peaks (2θ) appeared at 39.1º, 47.2º and 68.3º, are corresponding to the {111}, {200} and {220} planes of fcc Pd (JCPDS 05-0681). It is worthy to note that the PdSPs are containing more {111} planes than {200}, suggesting that the Pd spindle-like structures grew along the {111} direction. Also, no peaks were present for the Pd impurities which shows the high purity of the as-prepared PdSPs [**39**]. A sharp diffraction peak was appeared at 2θ = 12.6 and 22.3º and is attributed to the characteristic (110) and (020) plane of CMF [**40**]. The diffraction peaks at 10.8º are corresponding to the (002) plane of GO [**41**]. The other diffraction peaks appeared in **Fig. 1A** is related to the ITO substrate. The XRD results

confirmed the formation of GO-CMF/PdSPs composite.

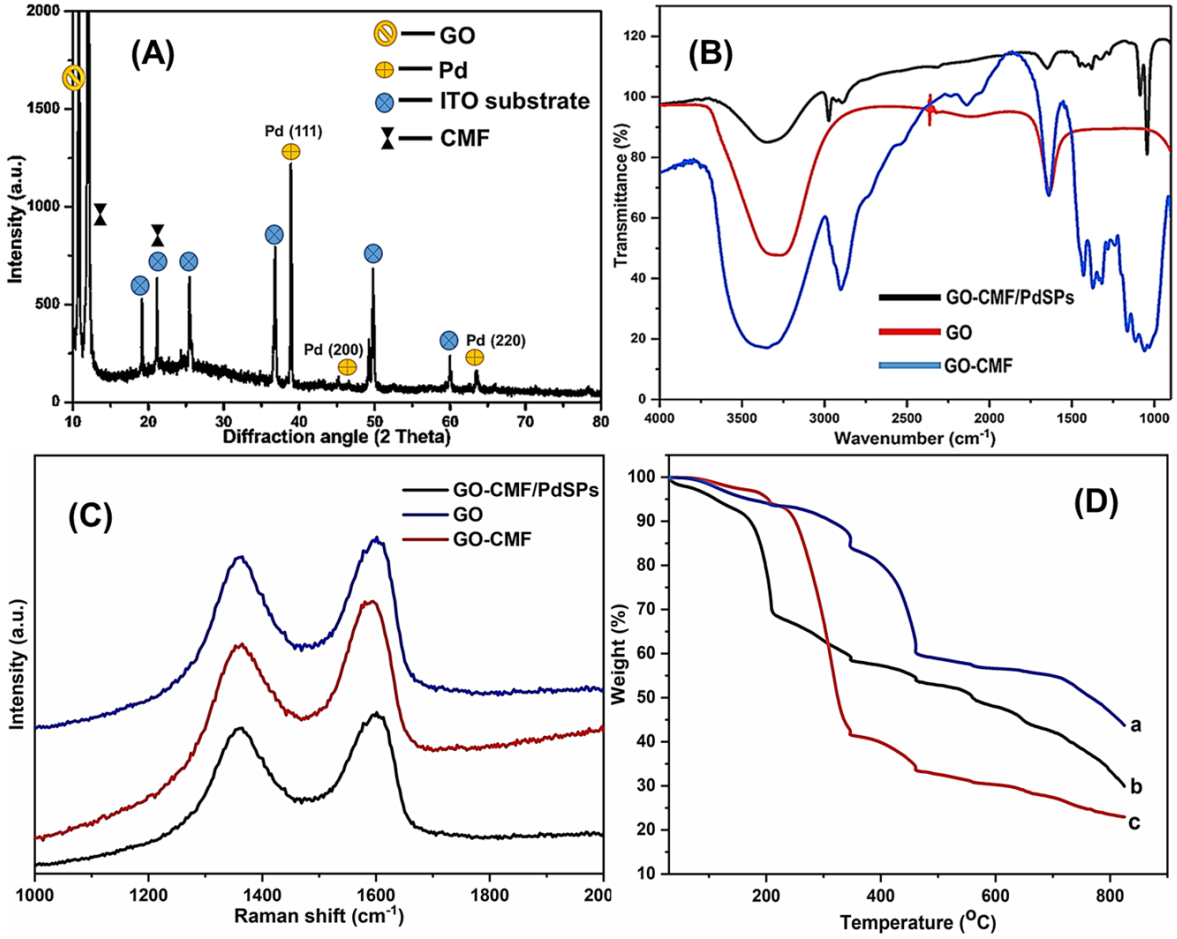

Figure 1 A) XRD spectrum of GO-CMF/PdSPs composite. B) FTIR spectra of GO, CMF, and GO-CMF/PdSPs composite. C) Raman spectra of GO, GO-CMF, and GO-CMF/PdSPs composite. D) TGA curves of CMF (a), GO (b) and GO-CMF (c).

The FTIR is a sensitive and most preferred technique, has been widely used for the identification of functional groups and study the interaction of molecules in the composite. **Fig. 1B** shows the typical FTIR spectra of GO, CMF, and GO-CMF/PdSPs composite. The FTIR spectra of GO-CMF composite shows five distinct vibrational bands, namely O–H stretching (3410 cm^{-1}), asymmetric and symmetric CH_2 stretching (2969 and 2884 cm^{-1}), -CH2-CH_3 starching (1512 cm^{-1}), (C=O carbonyl stretching (1652 cm^{-1}) and C–O epoxy stretching (1072 cm^{-1}). On the other hand, GO shows broadband at 3360 cm^{-1}, which attributed to the O–H stretching vibrations of hydroxyl groups. In addition, an additional vibration band was appeared at 1635 cm^{-1} and is due to the C=O carbonyl stretching of COOH group in GO. The above

result confirms the presence of oxygen moieties in the as-synthesized GO. It is worthy to note that the vibration bands related to the CMF did not change upon introduction of GO, while the enhancement of O–H, $–CH_2$-CH_3, and C=O vibrations were observed in the FTIR spectrum of GO-CMF/PdNPs. The result confirms the formation of GO-CMF composite via hydrogen bonding between CMF and GO.

Fig. 1C shows the typical Raman spectra of GO (blue profile), GO-CMF composite (red profile) and GO-CMF/PdNPs (black profile). The investigated all synthesized materials show a typical D and G bands around 1355 and 1598 cm^{-1}, respectively. The I_D/I_G of GO (0.97) and GO-CMF (0.96) is found be similar. On the other hand, the I_D/I_G of GO-CMF/PdNP slightly decreased to 0.94, which is resulting from the attraction of GO-CMF with Pd. The result confirmed that the in-plane activity of GO was not affected by either CMF or PdSPs, as reported early. **Fig. 1D** shows TGA curves of pristine CMF (a), GO (b) and GO-CMF (c). As can be seen that the GO tend to lose 34% of its initial weight at the temperature range of 160–200ºC, which is resulting from the elimination of oxygen-containing molecules from the surface of GO. It is worthy to note that the CMF (curve a) has lost only 15% of its initial weight at the temperature range of 160–200ºC. As can be seen from the TGA curve of GO-CMF, the thermal stability of GO has been improved in the presence of CMF. Hence, GO-CMF composite can be used as a base material for synthesis of nanomaterials.

The surface morphology of the as-prepared GO, GO-CMF, PdSPs, and GO-CMF/PdSPs composite is shown in **Fig. 2**. The scanning electron microscope (SEM) image of GO (A) revealed the wrinkled morphology as one can expect. However, the GO-CMF composite (B) showed the crumbled morphology where GO sheets enfolded the CMF. The high miscible nature of these materials is attributed to the strong interaction of hydroxyl groups of the CMF with hydroxyl groups of the GO. As shown in **Fig. 2C**, the spindle-like Pd nanostructures were seen on the SEM of PdSPs. It is noted that CMF is driven force for the formation of spindle-like Pd rather than Pd nanoparticles as reported early [**30**] (**Scheme 1**). The length and width of PdSPs were approximately 460 and 45 nm. The SEM image of GO-CMF/PdSPs composite (D) revealed that the nanostructure of PdSPs (blue arrow) was visible on the surface of GO-

CMF composite (black arrow), which confirms the formation of GO-CMF/PdSPs composite. The length and width of PdSPs on GO-CMF was 446 and 40 nm and is very consistent with the SEM image of PdSPs (C). The above discussions confirmed the successful formation of PdSPs on GO-CMF composite.

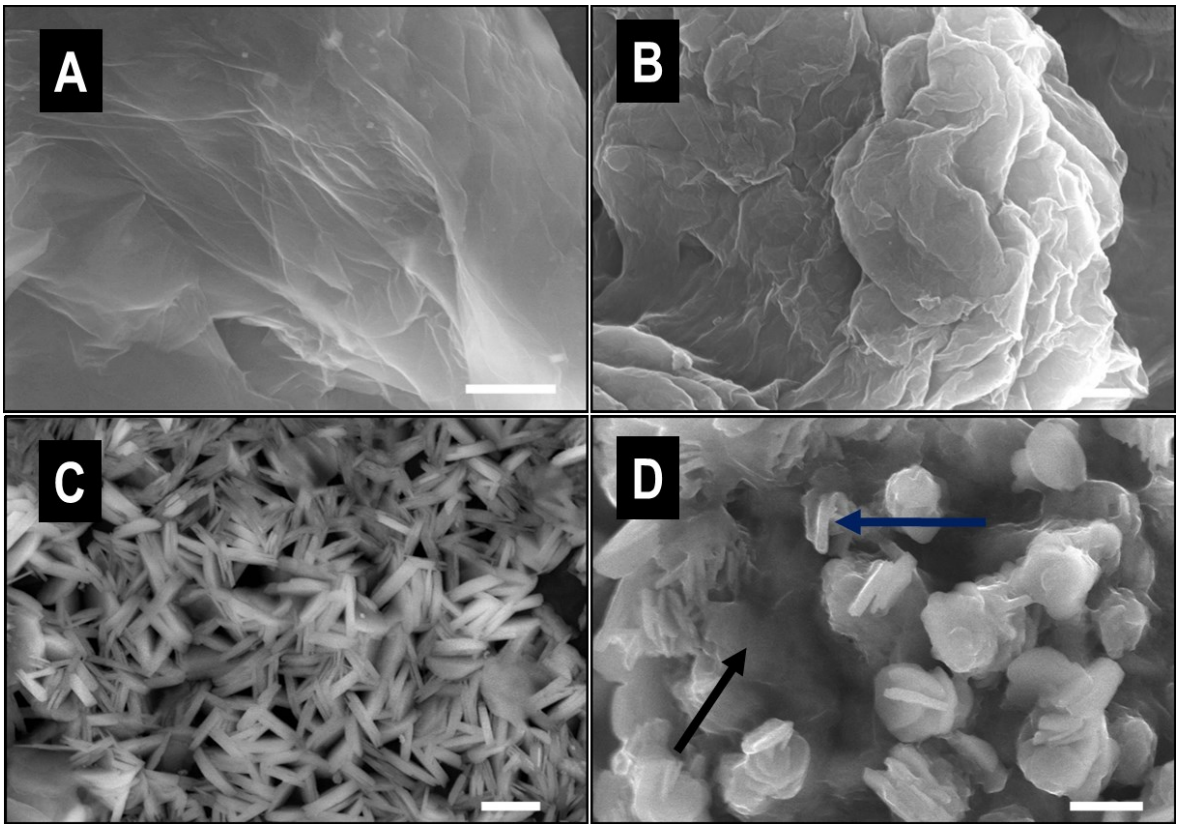

Figure 2 SEM images of GO (A), GO-CMF (B), PdSPs (C) and GO-CMF/PdSPs composite (D). Scale bar = 500 nm.

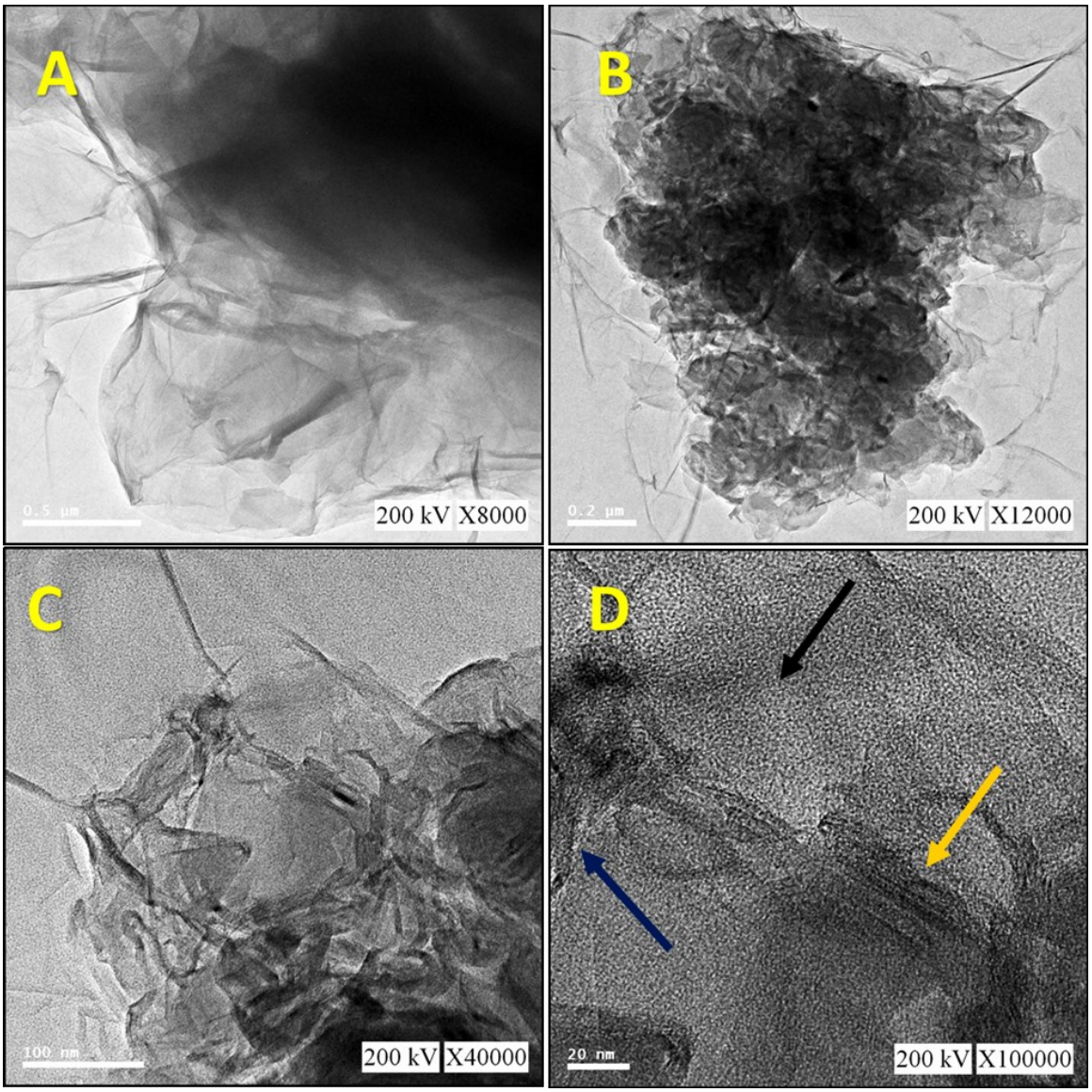

Figure 3 TEM images of GO (A), GO-CMF (B) and GO-CMF/PdSPs composite at lower and higher magnifications (C & D).

The morphological features of the as-synthesized materials were further confirmed using the images obtained from the transmission electron microscope (TEM). **Fig. 3** shows the TEM image of GO (A), GO-CMF (B) and GO-CMF/PdSPs composite (C & D). An ultra-thin sheet-like morphology appeared in TEM image of GO. A dense crumbled morphology was observed on the TEM picture of GO-CMF composite. The obtained morphological features are more consistent with the SEM image of GO and GO-CMF. The TEM image of GO-CMF/PdSPs composite (Fig. 3C) clearly shows a dense crumbled morphology of GO-CMF (blue and black arrows) and few spindles like Pd nanostructures (**Fig. 3D**, yellow

arrow). The results further confirmed the formation of GO-CMF and GO-CMF/PdSPs composites.

3.2. Electrochemistry of DA at CMF modified different composite electrodes

The electrochemistry of DA is already well-known for carbon nanomaterials modified electrodes, and the redox electrochemical behavior of DA is mostly quasi-reversible [**42**]. The redox electrochemistry of DA consists of the oxidation of DA to dopamine-o-quinone and the reduction of dopamine-o-quinone to DA [**42**]. Hence, the redox electrochemistry of DA at different modified electrodes was investigated by using cyclic voltammetry.

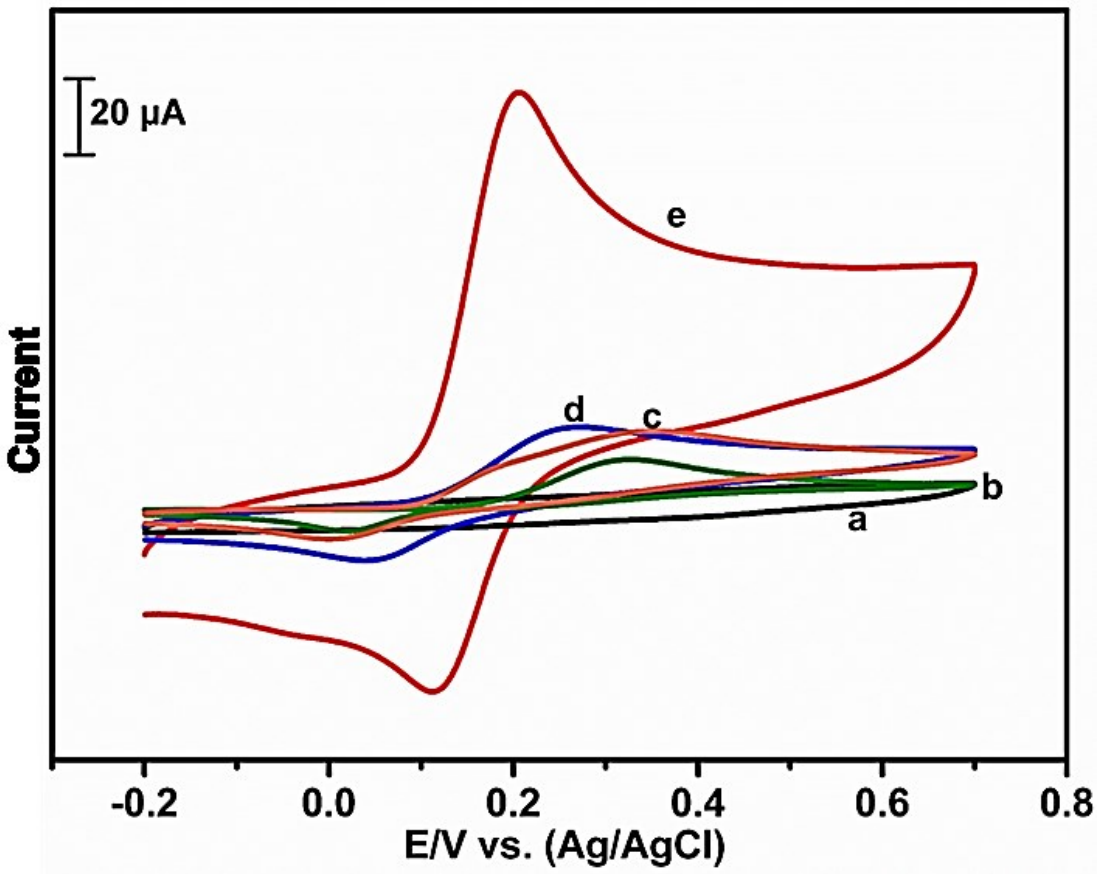

Figure 4 A) Cyclic voltammetry response obtained for bare GCE (a), GO/GCE (b), PdSPs/GCE (c), GO-CMF/GCE (d) and GO-CMF/PdSPs composite/GCE (e) in the electrochemical cell (pH 7.0) containing 50 µM DA at a scan rate of 50 mV/s.

The cyclic voltammetric experiments were performed in the potential sweeping from -0.2 to 0.7 V at a scan rate of 50 mV s^{-1}. The cyclic voltammetry response of different modified GCEs was tested in 10 µM DA containing pH 7.0, and the corresponding voltammograms are shown in **Fig. 4**. The unmodified

GCE (curve a) shows an insignificant anodic peak response to DA, and the irreversible anodic peak appeared at 0.345 V. While, the CMF modified GCE (curve b) shows a quasi-reversible and insignificant anodic (E_{pa}) and cathodic (E_{pc}) peak current response for DA. The E_{pa} and E_{pc} of DA appeared at 0.33 and 0.087 V, respectively. The peak-to-peak separation (ΔE_p, defined as $(E_{pa} + E_{pc})/2$) was found as 246 V. At the same conditions, PdSPs modified GCE (curve c) exhibited similar quasi-reversible behavior to DA, and E_{pa} and E_{pc} of DA appeared at 0.34 and 0.017 V, respectively. The calculated ΔE_p of DA at PdSPs/GCE is 77 mV higher than that of CMF/GCE. While the PdSPs modified GCE shows 1.3 folds higher anodic current response (I_{pa}) to DA than CMF/GCE. The E_{pa} of DA was observed at lower potentials when the electrode modified with GO (curve d), and E_{pa} and E_{pc} of DA were observed at 0.267 and 0.04 V, respectively. The obtained ΔE_p (227 mV) is 19 and 96 mV lower than those obtained for PdSPs and CMF modified GCEs. However, the obtained I_{pa} of DA is the same as those appearing at PdSPs. A well-defined quasi-redox couple with E_{pa} and E_{pc} of DA appeared at 0.207, and 0.107 V at GO-CMF/PdSPs composite modified GCE (curve e). The observed E_{pa} and E_{pc} of DA were 123, 133 and 29 mV lower than the response obtained for CMF, PdSPs and GO modified electrodes, which revealed the lower potential detection of DA. Also, the GO-CMF/PdSPs composite modified GCE shows 12 folds enhanced oxidation current response to DA than GO and PdSPs modified electrodes, which indicating the excellent electrooxidation ability of the composite modified electrode towards DA. It is worthy to note that the electrochemical redox behavior of DA is highly enhanced when the GO combined with CMF and PdSPs. The enhanced redox behavior and oxidation ability of the composite are due to the combined unique properties of GO-CMF with PdSPs. It is well-known that GO and CMF have abundant hydroxyl groups on their surface, and they can easily interact with DA by intermolecular hydrogen bonding. Furthermore, the excellent stability, high surface area to volume ratio, and electrochemical properties of PdSPs can accelerate the electrochemical oxidation of DA towards the electrode surface. Thus, these all combined properties are resulting in the enhanced electrochemical behavior of DA at the GO-CMF/PdSPs composite modified electrode than individual single compound electrodes.

The effect of scan rates on the redox electrochemical behavior of DA at the composite modified electrode was investigated. Cyclic voltammetry was used to evaluate the electrochemical redox behavior of DA at GO-CMF/PdSPs composite modified electrode and was examined in 10 µM DA containing pH 7.0 at different scan rates. The scan rates were tested in the range from 20 to 200 mV/s. The obtained cyclic voltammetric responses are shown in **Fig. 5A**.

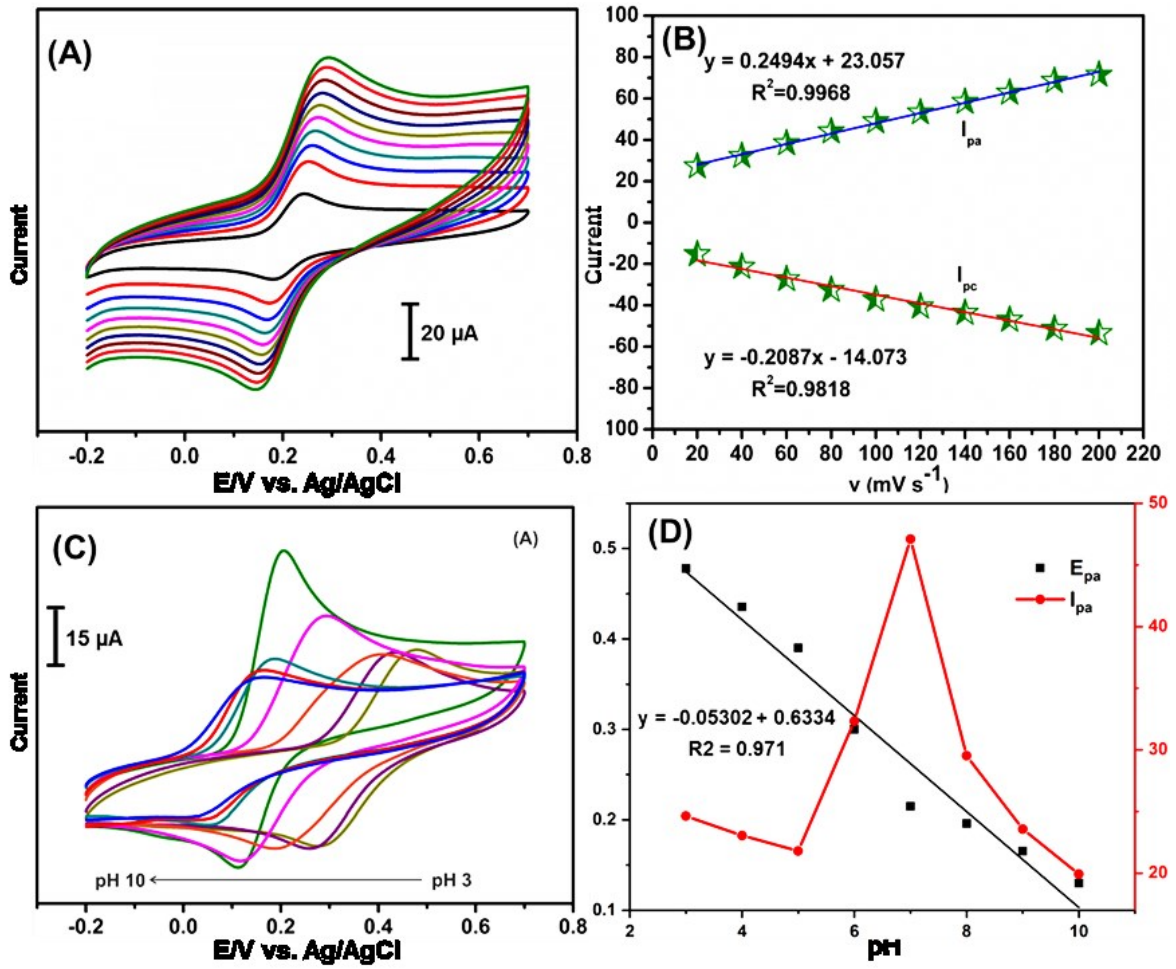

Figure 5 A) The effect of scan rate on the cyclic voltammetric response of GO-CMF/PdSPs composite modified GCE at 50 µM DA containing pH 7.0; the scan rate tested from 20 to 200 mV/s (inner to outer). B) The linear plot for the scan rate vs. anodic (I_{pa}) and cathodic (I_{pc}) current response. C) The voltammetric response of GO-CMF/PdSPs composite modified GCE at 50 µM DA containing different pH (pH 3 to 11) at a scan rate of 50 mV/s. D) Corresponding plot for pH vs. anodic peak potential (E_{pa}) and peak current (I_{pa}) of DA.

A well-defined quasi-reversible redox couple of DA was appeared for when the scan rate was 20 mV/s, and the I_{pa} and I_{pc} of DA increase with increasing the scan rates over 20 mV/s. It can also be seen that the E_{pa} and E_{pc} of DA slightly move towards positive and negative direction upon increasing the scan rates, which suggests that the mixed-kinetic reaction occurred for the redox electrochemistry of DA at higher scan rates. The calibration plot of scan rate against DA current response (**Fig. 5B**) has confirmed that the I_{pa} and I_{pc} of DA had a linear relationship with the scan rates from 20 to 200 mV/s. The linear equation can be expressed as E_{pa} (V) = 23.1v (mV/s) + 0.249 (R^2 = 0.9968) and E_{pc} (V) = 14.1v (mV/s) + 0.209 (R^2 = 0.9968). The above discussions revealed that the scan rates are linearly proportional to the I_{pa} and I_{pc}, and confirmed that the redox electrochemical reaction of DA at the modified electrode is an adsorption-controlled electrochemical process [4**2**].

The electrochemical redox behavior of DA was further examined in different pH since the electrochemistry of DA is pH dependent. Earlier studies have confirmed that the oxidized product of DA (dopamine-*o*-quinone) is highly stable in weak acidic and neutral conditions. **Fig. 5C** illustrates the cyclic voltammetric response of GO-CMF/PdSPs modified electrode in 10 μM DA containing different pH solutions (pH 3.0–10.0) at a scan rate of 50 mV/s. Each solution was saturated with N_2 by at least 3 min to removed the molecular oxygen from the solution. The composite modified electrode shows a clear redox couple for DA in different pHs. Furthermore, the I_{pa} and I_{pc} of DA were found the same in pH over and below 7.0. The E_{pa} and E_{pc} of DA shifted towards positive and negative direction upon increasing and decreasing of the pH. The result shows that the energetic protons/electrons transferred in redox electrochemical reaction of DA [**43**]. It is worthy to note that the I_{pa} and I_{pc} of DA were higher in pH 7.0 than other pHs (inset), which revealed that the composite modified electrode has a high catalytic activity to DA at pH 7.0. As shown in **Fig. 5D**, the E_{pa} of DA had a linear dependence on the pH ranging from 3.0 to 10.0, and the corresponding linear equation is E_{pa} (V) = −0.05302 V/pH + 0.6334, (R^2 = 0.971). The obtained slope value (-53.02 mV/pH) is closer to the reported theoretical value for the equal number of electrons and protons transferred electrochemical redox reaction. According to earlier studies, the DA

redox electrochemistry is involving two electrons, and protons transferred reversible reaction of DA to dopamine-*o*-quinone [**43**]. The possible electrochemical redox mechanism of DA at the GO-CMF/PdSPs modified electrode is shown in **Fig. 6**.

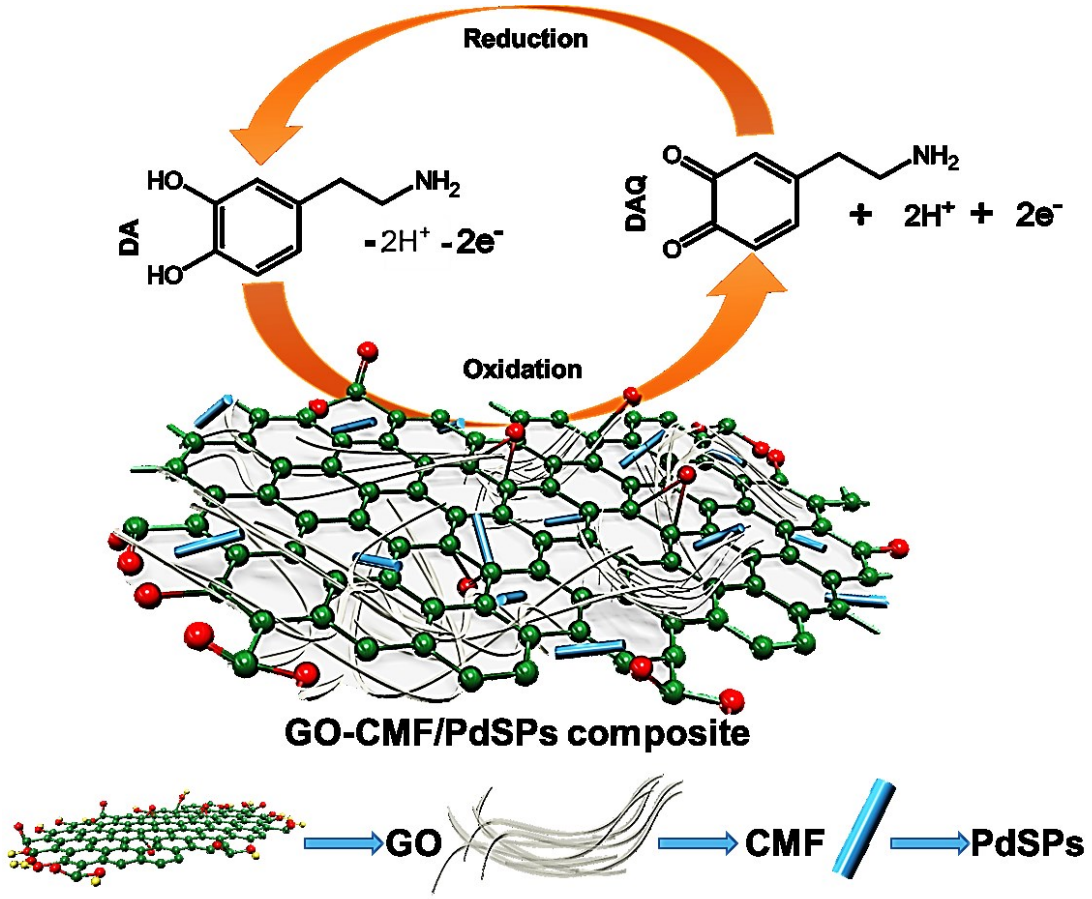

Figure 6 Scheme for electrochemical redox chemistry of DA at GO-CMF/PdSPs modified electrode.

3.3. Determination of DA and analytical merits

DPV was used for the sensitive determination of DA since it has higher analytical sensitivity and small background signal than cyclic voltammetry and linear sweep voltammetry. To optimize the sensor performance, we have studied the effect of accumulation time for the response to 1 μM DA since the electrochemical oxidation of DA at GO-CMF/PdSPs composite is an adsorption-controlled electrochemical process. The better sensitivity of DA observed for 60 s (not shown), and hence it is used as an optimum for further DPV measurements. The DPV measurements were carried out by using an initial E = -0.2 V, final E = 0.7 V, amplitude = 0.05 V, pulse width = 0.05 s, sampling width = 0.2 s and

pulse period = 0.2 s.

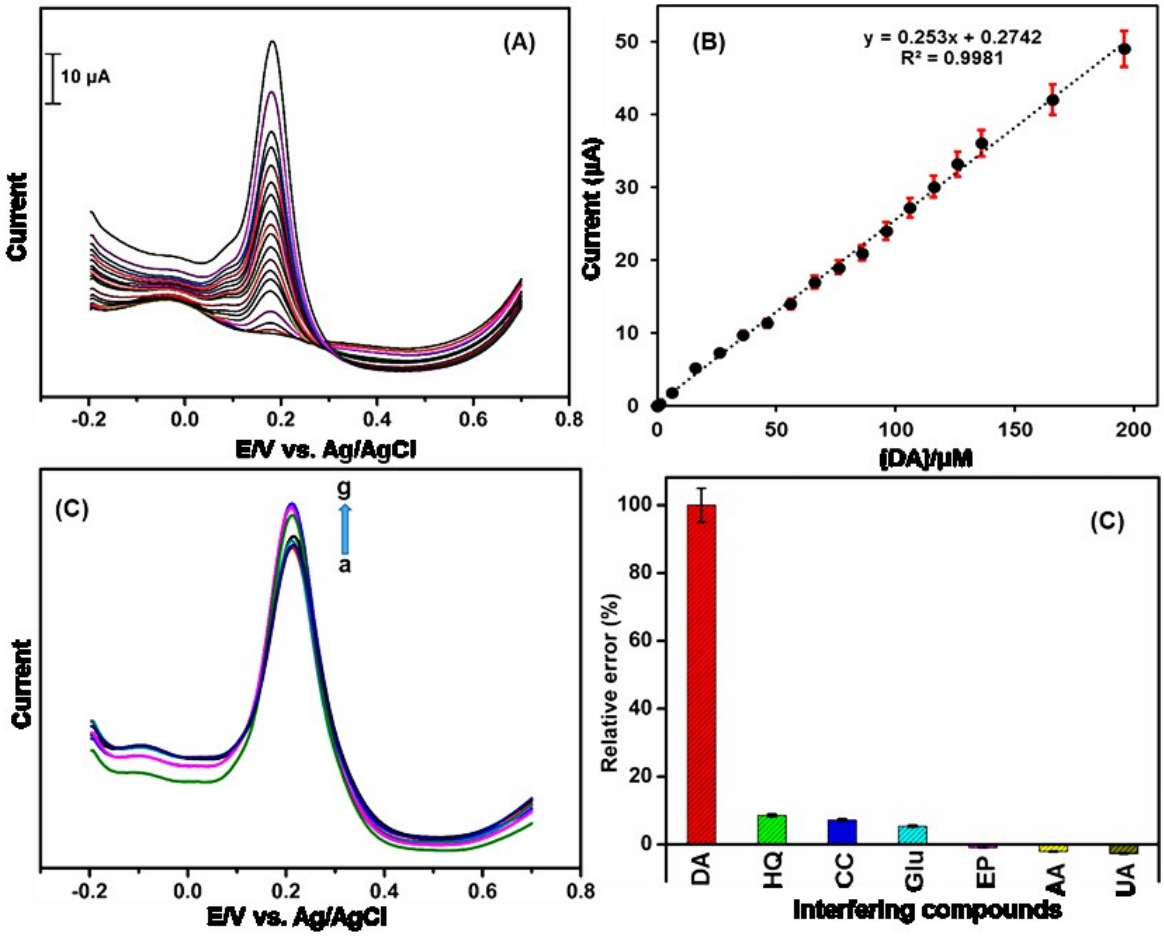

Figure 7 A) DPV responses of GO-CMF/PdSPs composite modified GCE for the absence and presence of different concentrations of DA (0.3 to 236.3 µM) at the pH 7.0. B) Calibration plot for [DA] vs. I_{pa} of DA. C) The effect of addition of 20 µM interfering compounds such as uric acid (a), ascorbic acid (b), epinephrine (c), glucose (e), catechol (f) and hydroquinone (g) on the DPV response of 1 µM DA (d) at GO-CMF/PdSPs composite modified GCE. D) The corresponding bar diagram for interfering compounds vs. relative response.

Fig. 7A shows the DPV response of GO-CMF/PdSPs composite electrode for the absence (initial DPV curve) and presence of DA (0.3 to 236.3 µM) in deoxygenated pH 7.0. In the absence of DA, the composite modified electrode did not show any apparent response in the scanned potential. The result shows that the composite modified electrode is electrochemically in-active in this potential window at pH 7.0. A clear DPV response was observed at 0.179 V for the addition of even the lower concentration of

(0.3 μM) DA (second curve), which indicates the excellent electro-oxidation of DA even at lower levels.

Table 1 The comparison of the analytical performances of the fabricated DA sensor with previously reported DA sensors based on Pd and its composites.

Sensor electrode	Detection method	LOD[a] (nM)	Linear range (μM)	Real samples	Ref.
[1]PdNPs/GCE	DPV[b]	–	8.0–88.0	DA injection	[**29**]
[2]RGO-PdNPs/GCE	LSV[c]	233.0	1.0–150.0	DA injection	[**30**]
[3]Pd/NPGW	DPV	–	1.0–220.0	Serum	[**35**]
[4]PdNPs/CNF/CPE	DPV	200.0	0.5–160.0	Human urine	[**36**]
[5]Pt/PF/Pd/GCE	DPV	48.2	0.5–100.0	Not tested	[**44**]
[6]AuNPs/PdE	SWV[d]	80.0	0.5–1000.0	pharmaceutical samples	[**45**]
[7]C60-PdNPs/SPCE	DPV	56.0	0.35–133.35	DA injection	[**46**]
[8]PdNPs/Silicon ITO	DPV	25.0	0.05–130.0	Not tested	[**47**]
[9]GR/GCE	DPV	2640.0	4.0–100.0	Not tested	[**48**]
[10]GO	Fluorescent	94.0	up to 2.0	Human urine and serum	[**49**]
[11]Au@Pd-RGO/GCE	DPV	24.0	0.01–100.0	Human urine	[**50**]
[12]PdAg NFs/rGO/GCE	DPV	48.0	0.4–96.0	Not tested	[**51**]
GO-CMF/PdSPs/GCE	DPV	23.0	0.3–196.3	DA injection and serum	This work

Abbreviations

[a]Limit of detection; [b]Differential pulse voltammetry; [c]Linear sweep voltammetry; [c]Squarewave voltammetry.

[1]Pd nanoparticles modified glassy carbon electrode; [2]Pd nanoparticles/reduced graphene oxide modified glassy carbon electrode; [3]Pd nanoparticles on self-supporting Au nanoporous wire; [4]Palladium nanoparticle-loaded carbon nanofibers modified carbon paste electrode; [5]Palladium nanoclusters-coated polyfuran modified Pt electrode; [6]Au nanoparticles coated Pd electrode; [7]Pd nanoparticles/C60 modified screen-printed carbon electrode; [8]Pd nanoparticles coated Si modified indium tin oxide; 9graphene modified glassy carbon electrode; [10]graphene oxide; [11]graphene oxide supported Au@Pd composite modified glassy carbon electrode; [12]porous bimetallic PdAg nanoflowers supported on reduced graphene oxide modified glassy carbon electrode

The DPV response increases with the addition of different concentration of DA (up to 236.3 μM). It

can be seen from the DPV profile that the response current of DA is linearly proportional to the concentration of DA. The calibration plot in **Fig. 7B** reveals that the electro-oxidation of DA at the GO-CMF/PdSPs composite electrode had a linear dependence with [DA] from 0.3 μM to 196.3 μM. The linear equation for current response vs. [DA] can be expressed as I_{pa} = 0.253 *C* + 0.2742, and R^2 = 0.9981. The sensitivity of the sensor was calculated as 253 μAμM^{-1}. The limit of detection of the sensor is 0.023 μM. The novelty and analytical performance of the present sensor are compared with previously reported DA sensors since different micro and nanocomposite material modified electrodes have already been used for the detection of DA in the recent decade. The analytical performances such as LOD, sensitivity and linear response range of the sensor are compared with previously reported Pd nanostructures, and its composite based DA sensors [**29, 30, 35, 36, 44-51**], and the comparative results are shown in **Table 1**. The comparison results revealed that the GO-CMF/PdSPs composite electrode had shown enhanced analytical features (lower LOD, wider response range) towards the determination of DA than other reported Pd nanostructured composites based DA sensors shown in **Table 1**. It is also worthy to note that the most of the works mentioned in **Table 1** do not use their sensor for the detection of DA in real samples, and some of them are a single real sample. The above discussions confirmed that the GO-CMF/PdSPs sensor electrode could be used as an alternative probe for the sensitive and low-level detection of DA.

The selectivity of the GO-CMF/PdSPs composite electrode was examined for detection of DA and other potentially interfering compounds such as hydroquinone (HQ), catechol (CC), glucose (Glu), epinephrine (EP), AA and uric acid (UA). **Fig. 7C** shows the DPV response of GO-CMF/PdSPs composite electrode for the presence of 1 μM DA (d) and 20 μM of UA (a), AA (b), EP (c), Glu (e), CC (f) and HQ (g) in pH 7.0. The DPV working parameters are same as in **Fig. 7A**. A clear DPV response was obtained for the presence of DA, and the changes in DPV response of DA were observed for DA with interfering compounds. However, the potential of DA was not affected by the additions of interfering compounds, revealing that these compounds did not have cross-reactivity with DA. The changes in the sensor selectivity (relative error) towards detection of DA are shown as a bar diagram in **Fig. 7D**. The presence

of HQ and CC caused significant changes (<4.6%) in the DA signal which is due to the closer oxidation potential and similar structural activity. However, other tested interfering compounds shows negligible reactivity (<3%) with the DA signal on the modified electrode. The reason may be due to the strong electrostatic interaction of positively changed DA on the composite electrode surface, reported previously [**37**]. The results confirmed that GO-CMF/PdSPs composite electrode could be used for selective detection of DA in the presence of tested interfering compounds. In addition, the high selectivity of the sensor could be more useful for the real-time detection of DA in pharmaceutical and biological samples.

Table 2. Real-time determination of DA levels in pharmaceutical and biological samples using as-prepared GO-CMF/PdSPs sensor electrode. RSD = 3 measurements.

Sample	Added (μM)	Found (μM)	Recovery (%)	RSD (%)
DA injection	0.5	0.486	97.2	3.9
	3.0	2.98	99.3	3.3
Human serum	0.5	0.472	94.4	4.8
	3.0	2.94	98.0	4.1

The practical applications of the GO-CMF/PdSPs composite electrode towards the determination of DA in pharmaceutical and biological samples were evaluated using DPV. The human serum is diluted with 10 mL of pH 7.0, and 1.0 mM of DA was added to the serum solution. The obtained human serum solution was used for the real sample analysis. 1.0 mM concentration of commercial DA injection solutions were prepared using pH 7.0 and used for the further analysis. The DPV was used to detect the known concentration containing human serum and DA injection solutions, and the recovery of DA was calculated using the standard addition method. The fabricated sensor was tested against the detection of different concentration addition (0.5 μM and 3 μM) of DA-containing DA injection and human serum solutions. The calculated recovery of DA in the real samples are tabulated in **Table 2**. The average recoveries of DA in the human serum and DA injection solutions were 96.2 and 98.3%, respectively. The obtained relative standard deviation (RSD) was below 5% for 3 measurements using the sensor modified electrode. The results confirmed that the GO-CMF/PdSPs composite sensor could be used for the accurate and

real-time detection of DA in pharmaceutical and biological samples.

The stability and reproducibility of the fabricated nanocomposite sensor electrode were evaluated using DPV. The GO-CMF/PdSPs electrode was used for the detection of 1 μM DA under optimum conditions. The stability of the sensor was examined up to 3 weeks, and the modified electrode was stored in dry condition when not in use. The sensor lost 8.9% of its initial sensitivity after 3 weeks' of storage (figure not presented). Also, the relative standard deviation (RSD) about 3.9% was found for 8 measurements of 1 μM DA using an independently prepared GO-CMF/PdSPs composite sensor electrode. The results confirmed the appropriate stability and reproducibility of the GO-CMF/PdSPs composite sensor.

4. Conclusions

In conclusion, we have prepared a PdSPs decorated GO-CMF composite using a simple electrochemical methodology. The SEM and XRD observations confirmed the formation of PdSPs on GO-CMF composite, and the FTIR spectrum of the composite confirmed the successful formation of GO-CMF composite. The combined synergistic effects of PdSPs with GO-CMF composite leads to the enhanced redox electrochemical behavior and sensitivity towards DA. The sensor showed promising analytical features towards the determination of DA, such as more extensive linear response ranges (up to 196.3 μM), nanomolar LOD with appropriate sensitivity. The sensor has a potential ability for selective detection of DA in the presence of possible interfering compounds such as HQ, CC, UA, and AA. The excellent practicality of the GO-CMF/PdSPs composite authenticates the promising nature of possible detection of DA in biological samples. As a future perspective, the as-synthesized PdSPs decorated GO-CMF composite the can be used for the fabrication of other electrochemical sensors and biosensors.

5. Conflicts of interest

We confirm that there are no conflicts to declare.

Acknowledgments

This project was supported by the Ministry of Science and Technology (project No: 106-2119-M-027-001) of Taiwan. This work was jointly supported by the Engineering and Materials Research Centre (EMRC), School of Engineering, Manchester Metropolitan University, Manchester, UK. Authors also would like to acknowledge the Precision analysis and Materials Research Center, National Taipei University of Technology for providing the all necessary Instrument facilities.

References

[1] V B. Mohan, K. Lau, D. Hui, D. Bhattacharyya, Composites Part B, 142 (2018) 200-220.

[2] Z. Liu, G. Wang, H.S. Chen, P. Yang, Chem. Commun., 54 (2018) 4720—4723.

[3] C. Jia, X. Zhang, K.M. Postolek, B. Huang, P. Yang, Carbon 139 (2018) 415–426.

[4] H. Chen, P.H. Chen, S.H. Huang, T.P. Perng, Chem. Commun., 50 (2014) 4379—4382.

[5] X. Huang, X. Qi, F. Boey, H. Zhang, Chem. Soc. Rev., 41 (2012) 666-686.

[6] L. Dong, J. Yang, M. Chhowall, K.P. Loh, Chem. Soc. Rev., 46 (2017) 7306-7316.

[7] R.K. Singh, R. Kumar, D.P. Singh, RSC Adv., 6 (2016) 64993–65011.

[8] A. Lerf, H. He, M. Forster, J. Klinowski, J. Phys. Chem. B, 102 (1998) 4477-4482.

[9] M. Pumera, Electrochem. Commun. 36 (2013) 14–18.

[10] L.G. Guex, B. Sacchi, K.F. Peuvot, R.L. Andersson, A.M. Pourrahimi, V. Ström, S. Farris, R.T. Olsson, Nanoscale, 9 (2017) 9562–9571.

[11] D. Chen, H. Feng, J. Li, Chem. Rev. 112 (2012) 6027−6053.

[12] Q. Huang, M. Xu, R. Sun, X. Wang, Ind. Crops Prod. 85 (2016) 198-203.

[13] A. Kafy, A. Akther, L. Zhai, H.C. Kim, J. Kim, Synth. Met. 223 (2017) 94-100.

[14] P. Balasubramanian, T.S.T. Balamurugan, S.M. Chen, T.W. Chen, T.W. Tseng, B.S. Lou, Cellulose, 25 (2018) 2381–2391.

[15] V. Velusamy, S. Palanisamy, S.M. Chen, T.W. Chen, S. Selvam, S.K. Ramaraj, B.S. Lou, Sens. Actuators, B 252 (2017) 175-182.

[16] S. Palanisamy, S.K. Ramaraj, S.M. Chen, T.C.K. Yang, P.Y. Fan, T.W. Chen, V. Velusamy, S. Selvam, Sci. Rep. 7 (2017) 41214.

[17] V. Velusamy, S. Palanisamy, S.W. Chen, S. Balu, T.C.K. Yang, C.E. Banks, Talanta 192 (2019) 471–477.

[18] S. Palanisamy, V. Velusamy, S.W. Chen, T.C.K. Yang, S. Balu, C.E. Banks, Carbohydr. Polym. 204 (2019) 152–160.

[19] P.R. Montague, S.E. Hyman, J.D. Cohen, Nature, 4 (2004) 760-767.

[20] M. Heien, A. Khan, J. Ariansen, J. Cheer, P. Phillips, K. Wassum, M. Wightman, Proc Natl Acad Sci USA 102 (2005) 10023-10028.

[21] J. Smythies, Neurotox. Res. 1 (1999) 27-39.

[22] M. Mallesh, R. Manjunath, C. Nethravathi, G.S. Suresh, M. Rajamathi, J.S. Melo, T.V. Venkatesh, Bioelectrochemistry, 81 (2011) 104-108.

[23] S. Liu, J. Yan, G. He, D. Zhong, J. Chen, L. Shi, X. Zhou, H. Jiang, J. Electroanal. Chem. 672 (2012) 40-42.

[24] Y. Wang, Y.M. Li, L.H. Tang, J. Lu, J.H. Li, Electrochem. Commun. 11 (2009) 889-892.

[25] M. Sajid, M.K. Nazal, M. Mansha, A. Alsharaa, S. Muhammad, S. Jillani, C. Basheer, TrAC 76 (2016) 15–29.

[26] K. Jackowska, P. Krysinski, Anal. Bioanal. Chem. 405 (2013) 3753–3771.

[27] S. Ku, S. Palanisamy, S.M. Chen, J. Colloid Interface Sci. 411 (2013) 182-186.

[28] B. Thirumalraj, S. Palanisamy, S.M Chen, R.S. Kannan, Electroanalysis 28 (2016) 425-430.

[29] S. Thiagarajan, R.F. Yang, S.M. Chen, Bioelectrochemistry 75 (2009) 163–169.

[30] S. Palanisamy, S. Ku, S.M. Chen, Microchim. Acta 180 (2013) 1037–1042.

[31] J. Li, J. Liu, G. Tan, J. Jiang, S. Peng, M. Deng, D. Qian, Y. Feng, Y. Liu, Biosens. Bioelectron. 15 (2014) 468–475.

[32] J. Wang, X. Chen, K. Liao, G. Wang, M. Han, Nanoscale Res Lett. 10 (2015) 311.

[33] Y. Xue, Y. Huang, Z. Zhou, G. Li, IOP Conf. Series: Mater. Sci. Eng 382 (2018) 022016.

[34] S. Dhanavel, T.A. Revathy, A. Padmanaban, V. Narayanan, A. Stephen, J. Mater. Sci. Mater. Electron. 29 (2018) 14093–14104.

[35] X. Yi, Y. Wu, G. Tan, P. Yu, L. Zhou, Z. Zhou, J. Chen, Z. Wang, J. Pang, C. Ning, Sci. Rep. 7 (2017) 7941.

[36] J. Huang, Y. Liu, H. Hou, T. You, Biosens. Bioelectron. 24 (2008) 632–637.

[37] F. Gao, X. Cai, X. Wang, C. Gao, S. Liu, F. Gao, Q. Wang, Sensors and Actuators B 186 (2013) 380–387.

[38] W.S. Hummers, R.E. Offeman, J. Am. Chem. Soc. 80 (1958) 1339.

[39] Y. Xu, J. Ma, Y. Xu, L. Xu, L. Xu, H. Li, H. Li, RSC Adv. 7 (2017) 2186–2192.

[40] N. Ma, D. Liu, Y. Liu, G. Sui, Int. J. Nanosci. Nanoeng., 2 (2015) 43-50.

[41] P. K. Sahoo, B. Panigrahy, D. Thakur, D. Bahadur, New J. Chem. 41 (2017) 7861-7869.

[42] S. Palanisamy, K. Thangavelu, S.M. Chen, P Gnanaprakasam, V. Velusamy, X.H. Liu, Carbohydr. Polym. 151 (2016) 401-407.

[43] Q.L. Zhang, J.X. Feng, A.J. Wang, J. Wei, Z.Y. Lv, J.J. Feng, Microchim. Acta 182 (2015) 589–595.

[44] N.F. Atta, M.F. El-Kady, A. Galal, Sensors and Actuators B 141 (2009) 566–574.

[45] S.K. Yadav, Rosy, M. Oyama, R.N. Goyal, J. Electrochem. Soc. 161 (2014) H41-H46.

[46] S. Palanisamy, B. Thirumalraj, S.M. Chen. M.A. Ali, F.M.A. Al-Hemaid, J. Colloid Interface Sci. 448 (2015) 251–256.

[47] C. Alexander, K. Bandyopadhyay, Inorg. Chim. Acta 468 (2017) 171–176.

[48] Y.R. Kim, S. Bong, Y.J. Kang, Y. Yang, R.K. Mahajan, J.S. Kim, H. Kim, Biosens. Bioelectron. 25 (2010) 2366–2369.

[49] J.L. Chen, X.P. Yan, K. Meng, S.F. Wang, Anal. Chem. 83 (2011) 8787–8793.

[50] J. Jiang, X. Du, Nanoscale, 6 (2014) 11303–11309.

[51] L.X. Chen, J.N. Zheng, A.J. Wang, L.J. Wu, J.R. Chen, J.J. Feng, Analyst, 140 (2015) 3183–3192.